Electronic Supplementary Information (ESI)

Boosting visible light harvesting and photocatalytic activity in surface modified TiO_2 photonic crystals by CoO_x nanoclusters

Alexia Toumazatou, [a] Maria Antoniadou, [b] Elias Sakellis, [b] Dimitra Tsoutsou, [b] Spyros Gardelis, [a] George Em. Romanos, [b] Nikolaos Ioannidis, [b] Nikolaos Boukos, [b] Athanassios Dimoulas, [b] Polycarpos Falaras, [b] and Vlassis Likodimos*[a]

[a] *Section of Condensed Matter Physics, Department of Physics, National and Kapodistrian University of Athens, Panepistimiopolis, 15784, Greece. E-mail: vlikodimos@phys.uoa.gr*
[b] *Institute of Nanoscience and Nanotechnology, National Center for Scientific Research "Demokritos", 15341 Agia Paraskevi, Athens, Greece*

S1. Materials characterization

The films morphology was characterized using a FEI Quanta Inspect scanning electron microscope coupled with energy-dispersive X-ray analyzer (EDX). The structure and phase composition of the PC films was studied by a FEI CM20 high-resolution transmission electron microscope (HR-TEM) equipped with a Gatan GIF 200 Energy Filter and a FEI Talos F200i S/TEM operating at 200 keV. The structural properties were investigated by micro-Raman spectroscopy using a Renishaw inVia Reflex microscope with a solid state laser and a laser diode emitting at 514 and 785 nm, respectively. The laser beam was focused onto the samples by means of a ×50 (numerical aperture NA=0.75) objective, while the laser power density was kept at low levels (0.05 $mW/\mu m^2$) to avoid local heating effects. In addition, laser annealing experiments were carried out by focusing the 785 and 514 laser beams on the surface of the CoO_x modified PC films by a 100× objective (NA=0.90) at full power of 60 and 2.5 mW, respectively and variable times up to 60 s in order to investigate the local oxidation of CoO_x deposits to the stable Co_3O_4 spinel phase. Normal Raman spectra were then acquired on the same spot at low laser power (0.05 $mW/\mu m^2$) to identify the local CoO_x structural phase transformation.

Low-pressure nitrogen (77.4 K), adsorption measurements were performed on an Autosorb 1-MP volumetric system (Quantachrome Inc. USA), with Krypton upgrade using approximately 5-10 mg of powder samples scraped from several inverse opal films, while the measuring temperature was fixed by means of a dewar flask containing liquid nitrogen. Ultra-high purity N_2 (99.999%), was used for all adsorption measurements, while He (99.999%) was used for volume calibrations. Prior to analysis, the samples were outgassed for 24 hours at 160 ^oC under high vacuum. The surface area was evaluated utilizing the multipoint BET (Brunauer Emmet Teller) method. The pore size distributions (PSDs) of the hierarchical meso-macroporous periodic structures in the inverse opal films were obtained from NLDFT analysis using the N_2 - silica adsorption branch kernel at 77 K

based on a cylindrical pore model for pores of diameter < 5nm, and spherical pores of diameter > 5nm. The mean pore size (d_{mean}) for spherical pore geometry was calculated by the total pore volume (TPV) at P/P_0=0.995 and the BET surface using the equation d_{mean}=6·(TPV)/(BET).

The optical spectra of the PC films were recorded on an Agilent Cary 60 UV-Vis spectrophotometer equipped with a Xenon flash lamp (80 Hz) in the range of 200-1000 nm. Diffuse reflectance spectra were acquired using the Agilent Cary 60 remote diffuse reflectance accessory (spot size of ~2 mm^2), while specular reflectance measurements were obtained at 15° utilizing a slide mounted accessory (PIKE, UV-Vis 15Spec). Baseline reflectance spectra were acquired by a Halon standard and a UV Al mirror, respectively. The stop band positions were estimated by modified Bragg's law for first order diffraction from the (111) *fcc* planes [1]:

$$\lambda = 2d_{111}\sqrt{n_{eff}^2 - \sin^2\theta},$$

where λ is the stop band wavelength, $d_{111} = \sqrt{\frac{2}{3}}\,D$ is the spacing between (111) planes, D is the macropore diameter and $n_{eff}^2 = n_{\mathrm{void}}^2 f + n_{\mathrm{TiO_2}}^2(1-f)$ is the volume-weighted average of the void spheres' refractive index, n_{void}, and titania $n_{\mathrm{TiO_2}}$, occupying the inverse opal frame, with f being the filling fraction ($f = 0.74$ for the ideal *fcc* lattice) and θ being the angle between the incident beam and the plane normal. Using the experimental stop band wavelengths at $\theta = 15°$ along with the measured diameters for $n_{\mathrm{TiO_2}} = 2.55$ and $n_{\mathrm{air}} = 1.0$, the n_{eff} values and filling fractions (1-f) were determined in air, as summarized in Table 1. In addition, using the obtained filling fractions and $n_{\mathrm{H_2O}} = 1.33$, the stop band positions were estimated for the PC films in water (Table 1), where the photocatalytic reaction takes place.

Photoluminescence (PL) measurements were carried out using the focused beam of a light-emitting diode at 275 nm for excitation and the PL signal was collected though a long-pass 320 nm cutoff filter by a fiber optic spectrophotometer (ASEQ Instruments-LR1). X-ray photoelectron spectroscopy (XPS) measurements were performed on a SPECS Phoibos100 instrument using a monochromatic Al Kα x-ray source (1486.6 eV) and a concentric hemispherical analyzer. The spectrometer was calibrated using clean silver, copper and gold samples. The $Ag3d_{5/2}$, $Cu2p_{3/2}$ and $Au4f_{7/2}$ peak positions were determined at be at 368.3 eV, 932.7 eV and 84 eV, respectively. The XPS spectra were collected at a measured angle θ_m=38° using a pass energy of 7 eV. Gaussian–Lorentzian shapes (Voigt functions) were used for deconvolution of the recorded photoelectron spectra after standard Shirley background subtraction.

Photoelectrochemical measurements were performed in a standard three-electrode system using an Autolab PGSTAT 302N potentiostat, a Pt foil as counter and Ag/AgCl as reference electrodes. The working electrode was prepared by the PC film assembly on cleaned fluorine-

doped tin oxide (FTO) transparent conductive glass electrodes (7 ohms/sq Pilkington) followed by the CCC surface modification in 1 mM $Co(acac)_2(H_2O)_2$ solution under the same conditions, described in Section 2.2. The electrolyte for the electrochemical measurements was 0.2 M Na_2SO_4, while visible light illumination was provided by a 300 W Xe lamp in combination with an AM 1.5 G filter for simulated solar light (100 mW/cm^2) and a 420 nm cutoff filter. Electrochemical impedance spectroscopy (EIS) measurements were carried out at open-circuit voltage, in the frequency range of 10^4–10^{-1} Hz with ac amplitude of 10 mV. The EI spectra were fitted to an equivalent circuit using a constant-phase element in parallel with the charge transfer resistance and a Warburg diffusion element, in order to take into account the non-homogeneity of the TiO_2 electrode, in series to an electrolyte solution resistance.

Electron paramagnetic resonance (EPR) measurements were carried out on an upgraded X-band Bruker ER-200D spectrometer interfaced to a personal computer and equipped with an Oxford ESR 900 cryostat, an Anritsu MF76A frequency counter and a Bruker 035M NMR gaussmeter. All room temperature EPR measurements were carried out using a perpendicular 4102ST cavity at 9.41 GHz with the following constant settings for the spin adduct detection: 20 mW microwave power, 8 mT scan range and 1 G field modulation. The formation of reactive oxygen species (ROS) by the prepared catalyst under visible light was investigated by scavenging the short lived ROS through their reaction with the nitrone DMPO, leading to characteristic nitroxide spin adducts. Scraped powder samples from the inverse opal films were suspended in DI water or acetonitrile (ACN) at a concentration of 1 mg/ml. DMPO was added to a final concentration of 0.1 M prior to visible light irradiation. Aliquots of at least 50 μl catalyst suspensions were placed in open ended capillary tubes with internal diameter of 0.9 mm that were then sealed at one end, and were inserted into 4 mm EPR quartz tubes. Visible light irradiation was applied outside the EPR cavity, prior to measurements, for various time intervals using a 360 W tungsten lamp. Subsequently, the samples were gently purged with N_2 for 30 s in order to decrease the concentration of dissolved O_2 that causes line broadening to the spin adduct EPR spectra. The isotropic EPR spectra were simulated using the EasySpin-5.2.27 software package [2] and the hyperfine coupling constants for the DMPO-ROS adducts reported in the literature [3].

S2. Photocatalytic performance

The photocatalytic activity of the PC and reference films was evaluated on the aqueous phase degradation of methylene blue (MB) (Alfa Aesar) and salicylic acid (SA) (Sigma-Aldrich) as model water pollutants under UV-Vis and visible light irradiation. The PC and reference films of 2 cm^2 area were placed horizontally at vials containing aqueous MB (4 mL, 3 μM) or SA (3 mL, 25 μM) aqueous solutions, where they were stirred for 60 min in the dark to reach adsorption–desorption

equilibrium, while SA adsorption was enhanced by stabilizing the solution pH at 3 by dilute HCl. The illumination source was a 150 W Xe lamp and UV-Vis irradiation was selected by a long-pass 305 nm cutoff filter and a heat reflective mirror (Newport 20CLVS-3 CoolView™). Visible light was selected by an additional long-pass 400 nm cutoff filter. The horizontal incident Xe beam was directed on the film via a UV-enhanced Al mirror (ValuMax, Newport) with power densities of 2.8 and 96 mW/cm^2 for the MB and SA degradation, respectively. Small (0.5 mL) aliquots of the pollutant solutions were periodically withdrawn and quantitatively analyzed using a 10 mm path length quartz microcell (HELMA Analytics) in the Cary 60 spectrophotometer. The photocatalytic experiments were performed in triplicate, and standard errors were calculated for the mean kinetic constants. Wavelength-dependent SA photodegradation tests were carried out for the CoO_x-1st-PC films under narrow band irradiation from three LEDs emitting at 405, 450 and 622 nm ($\pm$ 10 nm) and spectrophotometric detection using 3 mL 12 μM SA aqueous solutions (pH=3) after 60 min stirring in the dark. The stability of the photocatalytic films was tested by recycling three times the MB degradation test for the same film, with intermediate cleaning of MB residues by 1 hr UV-Vis illumination in 4 mL deionized water.

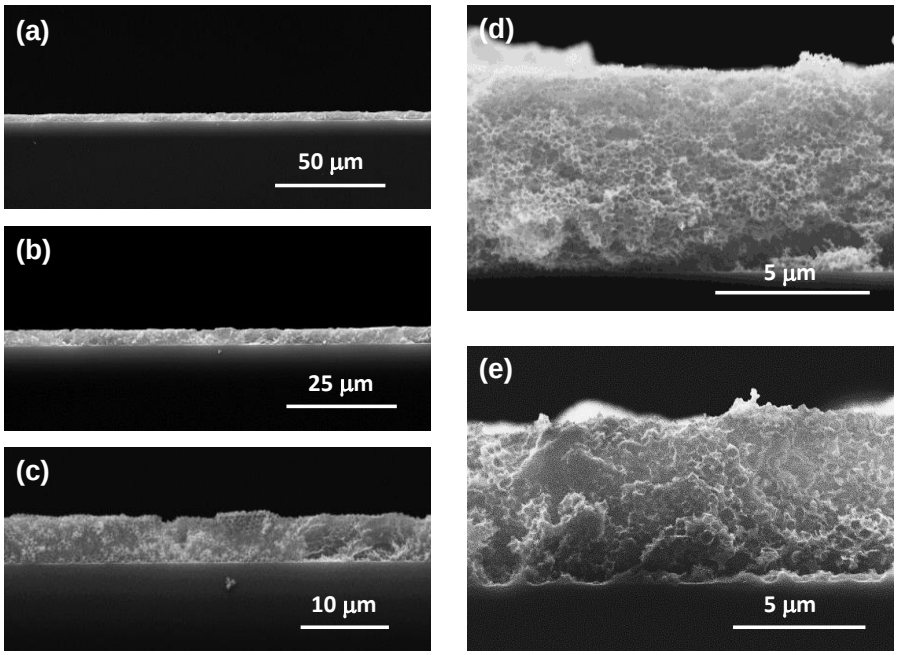

Figure S1. Cross section SEM images of the (a)-(c) PC260 films at different magnifications, (d) PC406 and (e) PC499 inverse opal films.

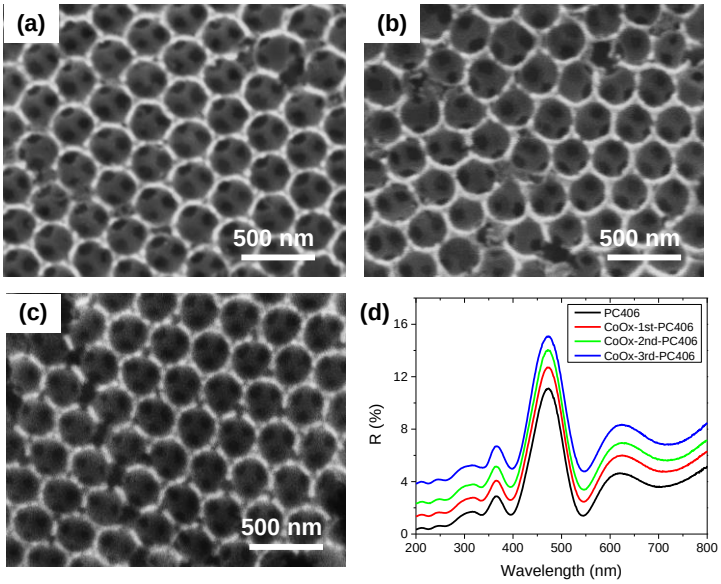

Figure S2. Top view SEM images for CoO_x-PC406 after the (a) 1st (b) 2nd, and (c) 3rd CC cycle and (d) the corresponding specular reflectance (R%) spectra at 15° incident angle.

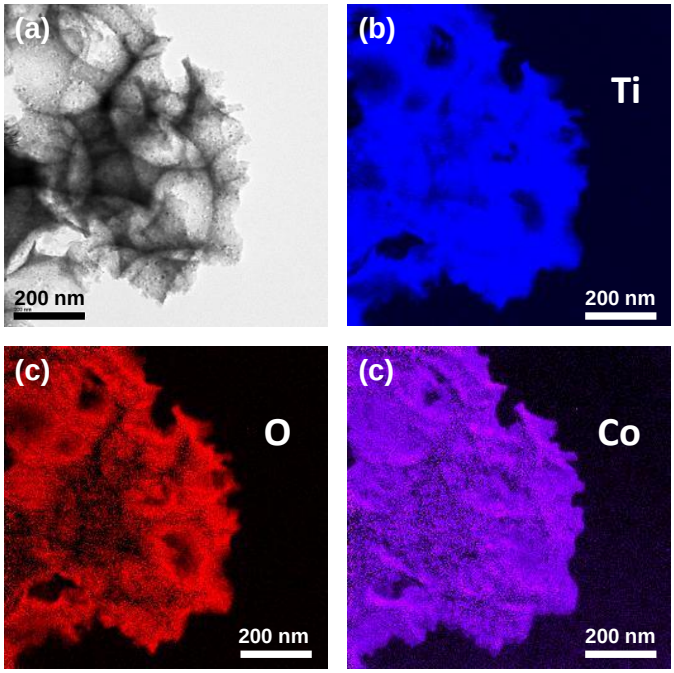

Figure S3. (a) Bright field TEM image for CoO_x-3rd-PC499 and the corresponding (b) Ti and (c) O and (c) Co EFTEM elemental maps.

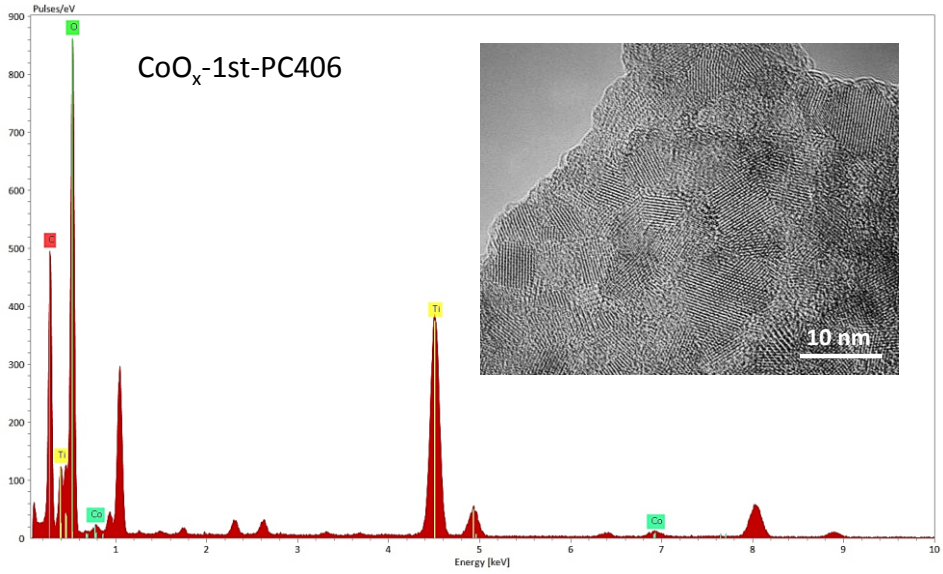

Figure S4. Local EDX spectrum for the area shown in the HR-TEM image for CoO_x-1st-PC406.

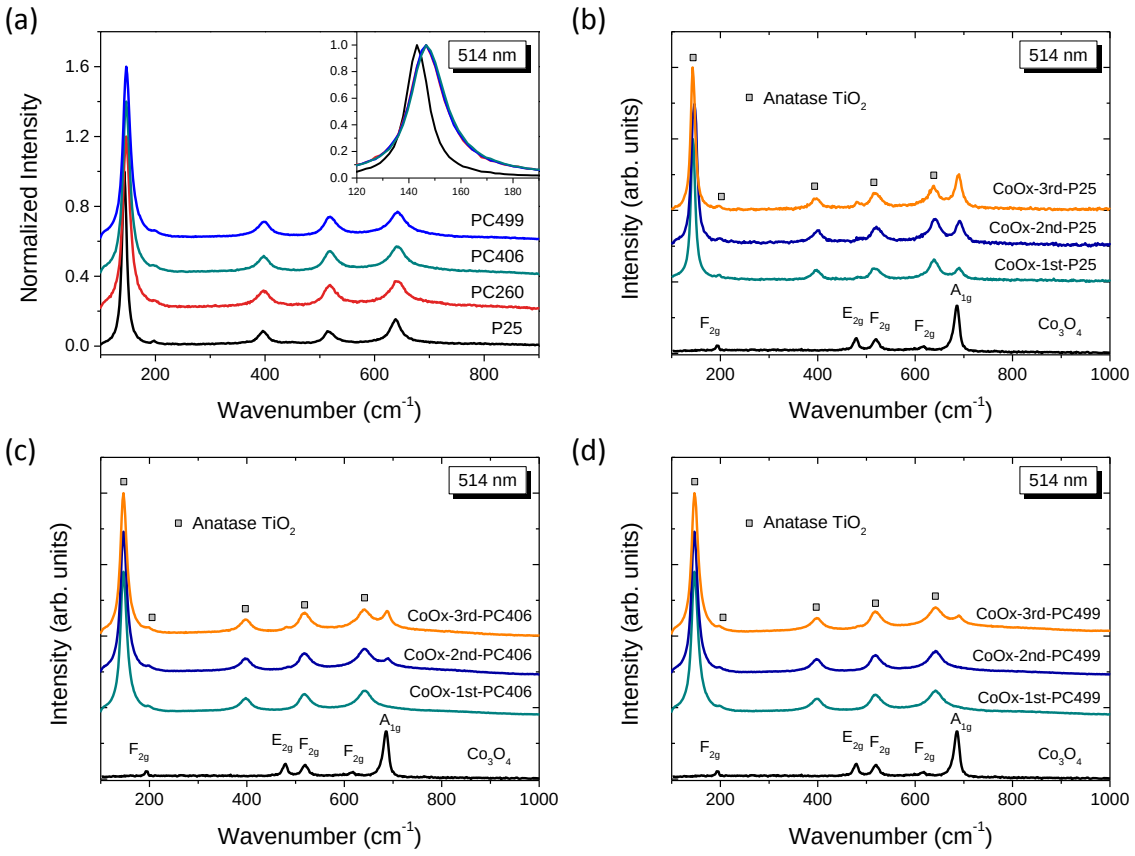

Figure S5. Micro-Raman spectra of the (a) pristine PC and P25 films at 514 nm. The inset compares the corresponding lowest frequency anatase E_g mode. Raman spectra variation with the CC modification cycles for (b) CoO_x-P25, (c) CoO_x-PC406, and (d) CoO_x-PC449 films in comparison with the reference spectrum of Co_3O_4 at 514 nm.

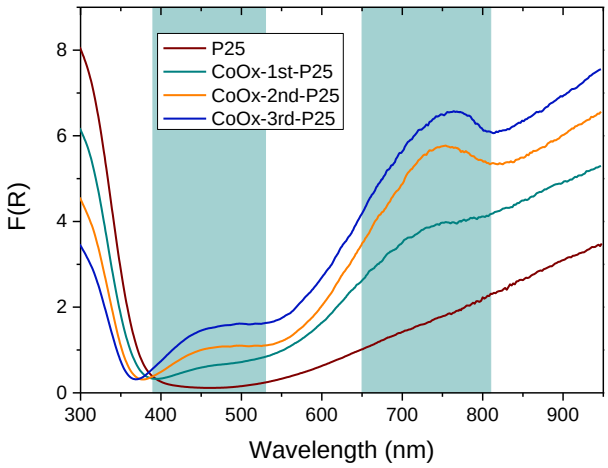

Figure S6. Kubelka-Munk transform function F(R) for the CoO_x-P25 films. The cyan-shaded areas indicate the Co_3O_4 electronic absorption bands.

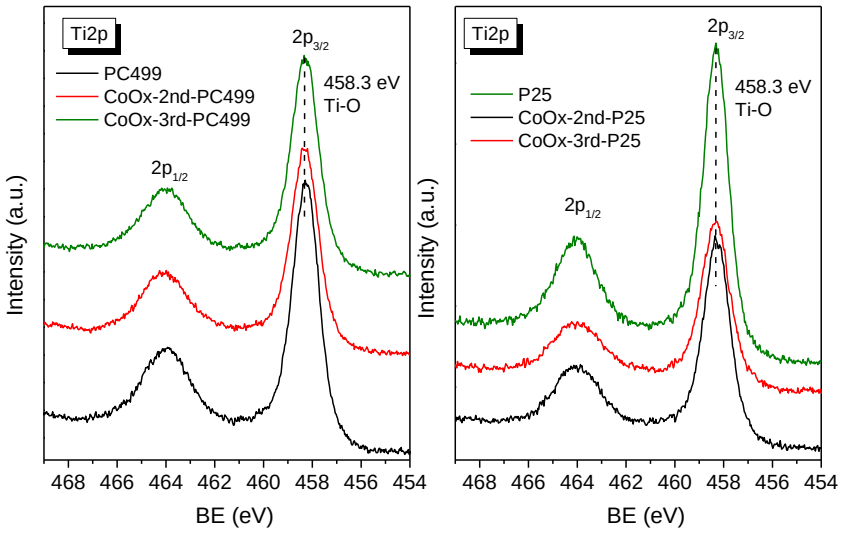

Figure S7. Ti 2p XP spectra for the pristine and CoO_x-modified PC499 and P25 films.

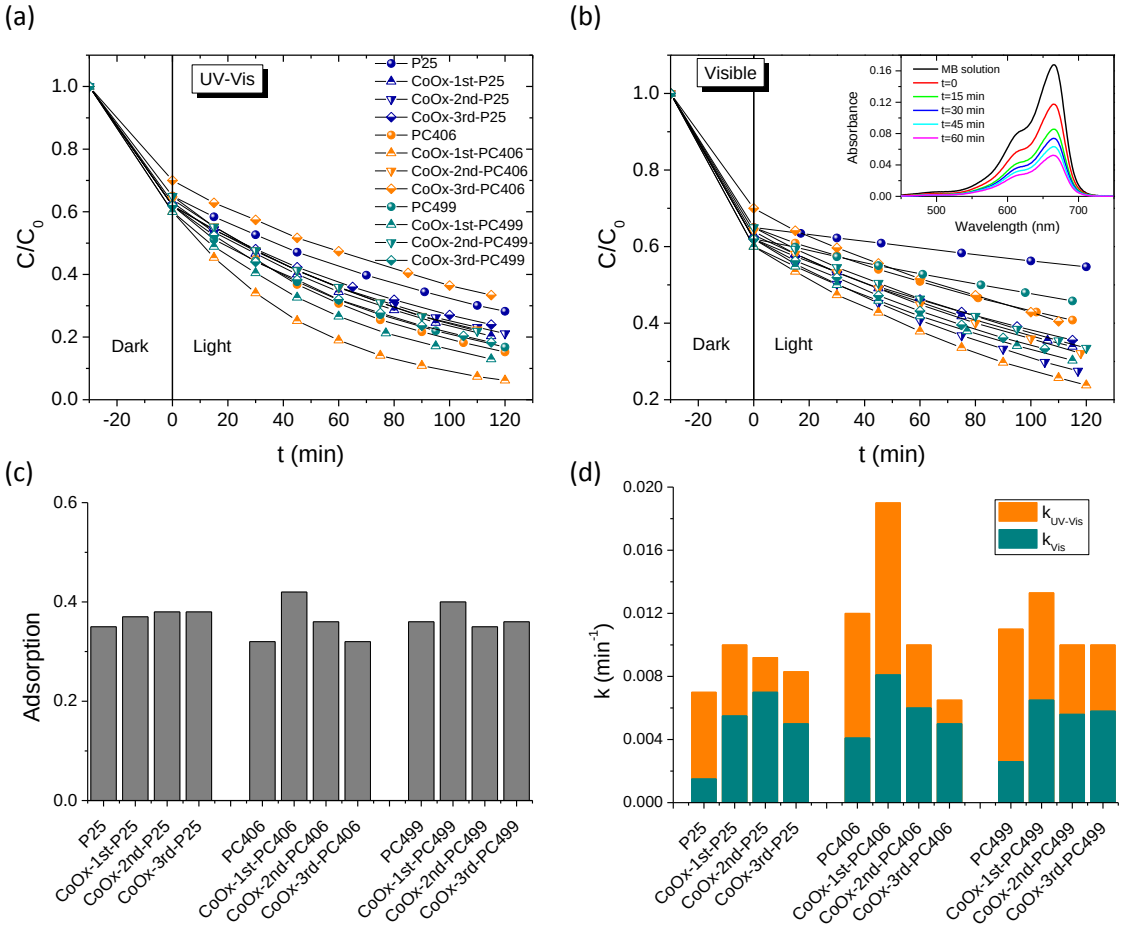

Figure S8. MB photodegradation kinetics for the CoO_x-modified inverse opal and reference P25 films under (a) UV-Vis and (b) visible light. (c) MB dark adsorption (%) and (d) apparent kinetic constants $k_{UV\text{-}Vis}$ and k_{Vis} for the different films. The inset in (b) shows the MB absorbance evolution for CoO_x-1st-PC406 under visible light.

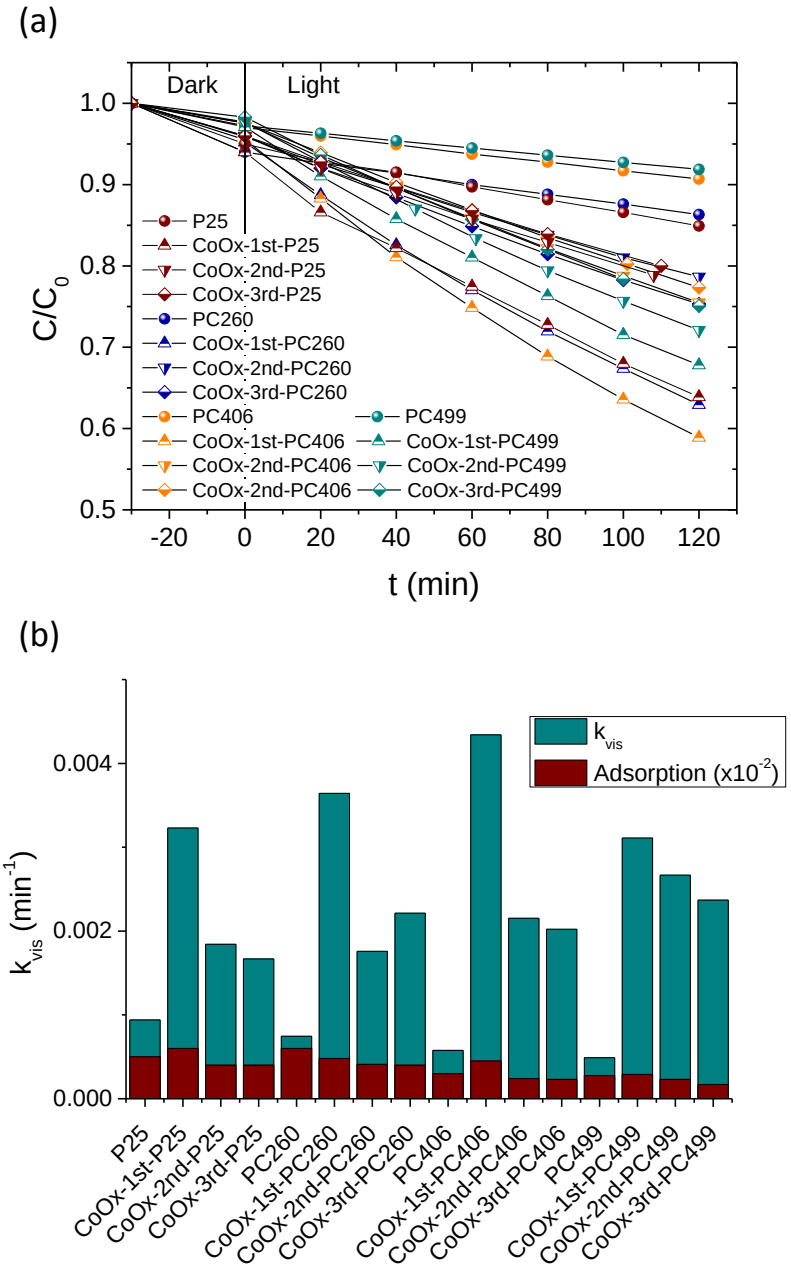

Figure S9. (a) SA photodegradation kinetics for the CoO_x-modified PC and P25 films under visible light and (b) the corresponding variation of the apparent kinetic constants k_{Vis} along with the SA dark adsorption (%).

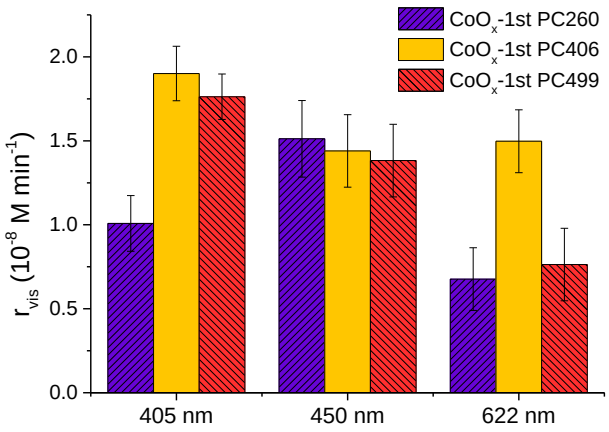

Figure S10. Wavelength-dependent reaction rates r_{Vis} for SA photodegradation by the CoO_x-1st-PC films under narrow band LED irradiation at 405, 450 and 622 nm.

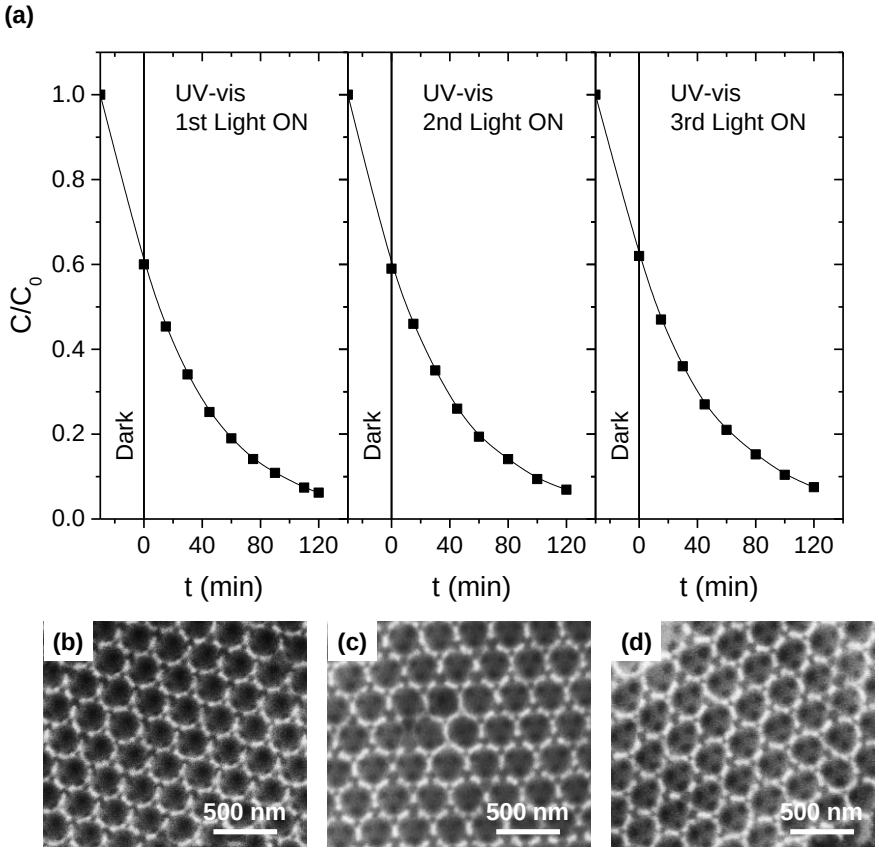

Figure S11. (a) Three successive MB photodegradation cycles using the same CoO_x-1st-PC406 film under UV-Vis illumination and (b), (c), (d) the corresponding SEM images of the film after each test.

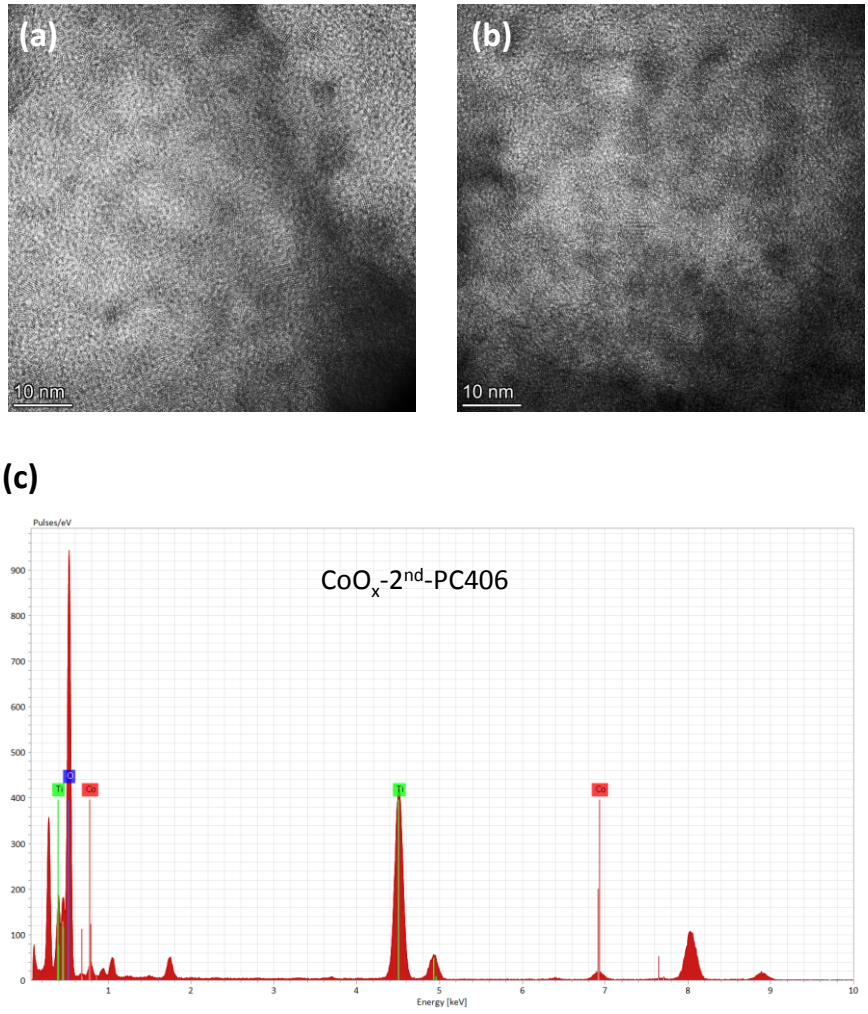

Figure S12. HR-TEM images for CoO_x-2nd-PC406 (a) before and (b) after the SA photodegradation test. (c) local EDX spectrum for the area shown in (b).

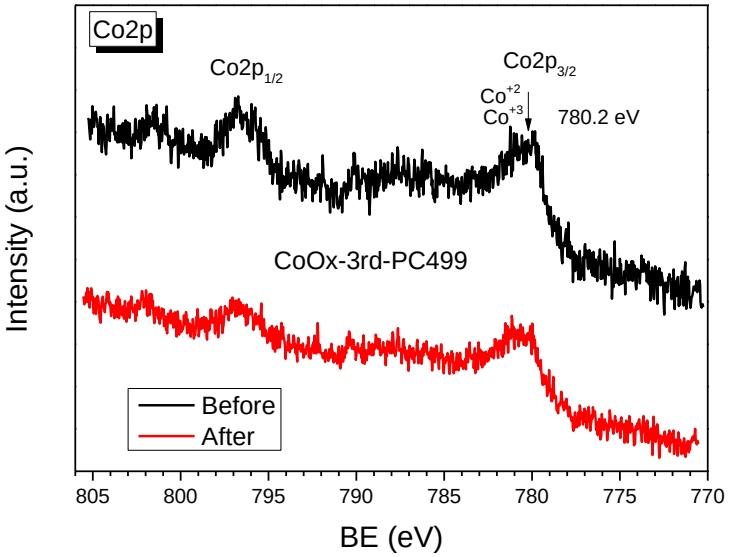

Figure S13. Co 2p XP spectra for CoO_x-3rd-PC406 before and after SA photodegradation.

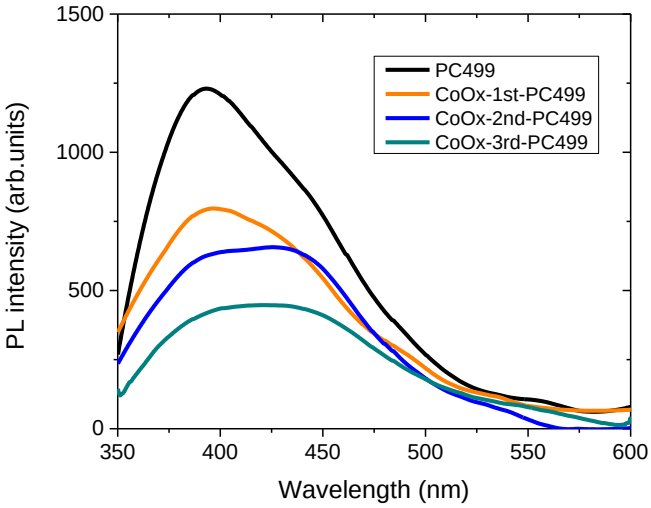

Figure S14. PL spectra for the CCC-modified PC499 films under 275 nm excitation.

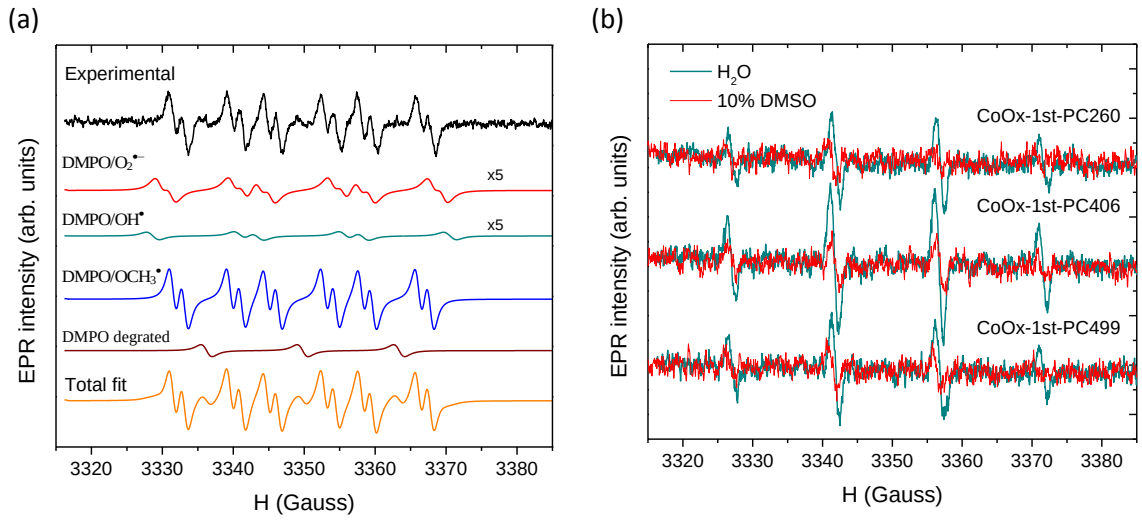

Figure S15. (a) Spectral deconvolution of the DMPO spin trap EPR spectra for PC406 1st suspensions in ACN after visible light illumination depicting the individual EPR spectral components of DMPO/$O_2^{\bullet-}$, DMPO/$OH^{\bullet}$, DMPO/$OCH_3^{\bullet}$ and degraded DMPO radical adducts. (b) Spin trap EPR spectra variation of DMPO/PC dispersions in water and in the presence of 10% dimethylsulfoxide (DMSO).

The small amount of DMPO/$OH^{\bullet}$ adduct detected can be ascribed to formation of $OH^{\bullet}$ from the following reactions of $O_2^{\bullet-}$ [4], which is produced from the reaction of conduction band electrons with dissolved O_2:

$O_2^{\bullet-} + H^+ \rightarrow HO_2^{\bullet}$ (1)

$2HO_2^{\bullet} \rightarrow H_2O_2 + O_2$ (2)

$H_2O_2 + O_2^{\bullet-} \rightarrow OH^{\bullet} + O_2 + OH^-$ (3)

$H_2O_2 + e^- \rightarrow OH^{\bullet} + OH^-$ (4)

$H_2O_2 + h^+ \rightarrow HO_2^{\bullet} + H^+$ (5)

Table S1. Elemental EDX analysis of the photonic and reference P25 films.

Samples	Ti (at %)	Co (at %)	Co/Ti
PC260 1st	95.53	4.47	0.047
PC260 2nd	93.98	6.02	0.064
PC260 3rd	90.65	9.35	0.103
PC406 1st	97.43	2.57	0.026
PC406 2nd	94.15	5.85	0.062
PC406 3rd	91.87	8.13	0.088
PC499 1st	97.57	2.43	0.025
PC499 2nd	95.05	4.95	0.052
PC499 3rd	93.05	6.95	0.075
P25 1st	96.48	3.52	0.036
P25 2nd	94.01	5.99	0.064
P25 3rd	90.76	9.24	0.102
PC406 1st after	97.46	2.54	0.026
PC406 2nd after	94.22	5.78	0.061
PC406 3rd after	92.01	7.99	0.087

References

[1] V. Likodimos, Photonic Crystal-assisted Visible Light Activated TiO_2 Photocatalysis. *Appl. Catal. B Environ.*, 2018, **230**, 269–303.

[2] S. Stoll and A. Schweiger, EasySpin a Comprehensive Software Package for Spectral Simulation and Analysis in EPR, *J. Magn. Reson.*, 2006, **178**, 42-55.

[3] D. Dvoranová, Z. Barbieriková and V. Brezová, Radical Intermediates in Photoinduced Reactions on TiO_2 (An EPR Spin Trapping Study). *Molecules*, 2014, **19**, 17279-17304.

[4] Y. Nosaka and A. Y. Nosaka, Identification and Roles of the Active Species Generated on Various Photocatalysts. In *Photocatalysis and Water Purification: From Fundamentals to Recent Applications*, 1st ed.; Pichat, P., Ed.; Wiley-VCH: Weinheim, Germany, 2013, 3–24.